Research Article

Chonlada Luangarpa*, Chaosuan Kanchanomai and Hideo Koguchi

Singularities at interface corners of piezoelectric-brass unimorphs

https://doi.org/10.1515/jmbm-2022-0254
received July 17, 2022; accepted September 14, 2022

Abstract: In this study, singularity fields at the interface corners of piezoelectric-brass unimorphs are investigated. Two models differing in side surface geometry (step and flat surfaces) are analyzed to study the singularity effect on mechanical (stress–strain) and electrical (electric potential and intensity) behavior. A mixed-mode mechanical boundary condition is applied for analyzing the realistic application of unimorphs, with normal force, shear force, and bending moment as internal forces. The conservative integral together with a three-dimensional finite element analysis is used to determine the intensity of singularity. There are three singularity terms at each vertex and singular line. All singularity terms are investigated in detail. Intensities of the singularities at the vertex and several points located on side surfaces (singular lines) are examined. Results show that the intensities of singularities for mixed-mode conditions differ from that of tensile load conditions. For mixed-mode conditions, the intensity of singularity must be calculated for all singularity terms. In addition, the stress singularity characteristics at the vertex may be described as a function of the singularities along the singular lines. These findings clarify the understanding of singularity at interface corners of piezoelectric-brass unimorphs and may be used as references for developing relevant piezoelectric devices.

Keywords: piezoelectric, bonded joints, unimorph, intensity of singularity, conservative integral

*** Corresponding author: Chonlada Luangarpa,** Department of Mechanical Engineering, Faculty of Engineering, Thammasat University, 99 Village No.18 Phahonyothin Road, Khlong Luang, Pathum Thani 12121, Thailand, e-mail: lchonlad@engr.tu.ac.th
Chaosuan Kanchanomai: Department of Mechanical Engineering, Faculty of Engineering, Thammasat University, 99 Village No.18 Phahonyothin Road, Khlong Luang, Pathum Thani 12121, Thailand, e-mail: kchao@engr.tu.ac.th
Hideo Koguchi: Department of Mechanical Engineering, Niigata Institute of Technology, 1719 Fujihashi, Kashiwazaki City, Niigata 945-1195, Japan, e-mail: hkoguchi@niit.ac.jp

1 Introduction

Piezoelectric materials, especially PZT (lead zirconate titanate), are used in numerous engineering and technological applications due to their unique properties [1]. Piezoelectric bonded joints (for example, bonded joints between PZT and brass) may be found in different devices, including transducers and sensors. At the bonded joints, stress singularity usually occurs as a result of mismatching of material properties across the interfaces. As it is known, a piezoelectric effect is a property related between mechanical pressure and electric charge; that is, besides mechanical stress singularities, singularity characteristics of the piezoelectric materials might affect electric fields.

There are several studies on the singularity behavior of piezoelectric materials on cracks [2–6] and bonded joints [7–14]. Those studies revealed that the singularity of the piezoelectric materials affects electric fields; therefore, it is more complicated to analyze the singularities of the piezoelectric materials than that of non-piezoelectric materials. For piezoelectric bonded joints, most studies focus on analyzing the order of singularity [7–11,13]. To clearly understand singularity behavior, the intensity of singularity is an important parameter in addition to the order of singularity. However, few studies have analyzed the intensity of singularity [12,14].

Recently, Luangarpa and Koguchi [15,16] focused on the investigation of the intensity of singularity of the piezoelectric bonded joints. These studies revealed that a magnitude of electric displacement increases as it approached the vertices, as with stress singularity. The concentration of electric displacements might cause an enlarged electric field. However, it is not clear how an electrical singular affects overall mechanical-electrical behavior.

Although the previous studies deal with the investigation of the intensities of singularities, all cases are applied tensile loading only. There remains a need for analysis of the mixed-mode boundary conditions (mixed between tensile and shear loading) since various applications of the piezoelectric material might be used in the

mixed-mode conditions, *e.g.*, an unimorph or a bimorph used for actuation, sensing, or energy harvesting.

The present study applied numerical methods to analyze a realistic case of the piezoelectric bonded joints. The unimorphs consisting of PZT (transversely isotropic piezoelectric material) and brass (isotropic material) are investigated. With unimorph application as a cantilever beam, internal forces comprised normal force, shear force, and bending moment (the mixed-mode condition). Furthermore, to our knowledge, no study on the singularity at the bonded joint between PZT and brass, which is a conductive material, has been conducted. In this study, the singular fields at a vertex and along the singular line of three-dimensional models are examined in detail. Two models differing in side surface geometry are analyzed to study the effect of singularity on mechanical (stress–strain) and electric (electric potential and intensity) behaviors. Each vertex and each singular line consist of three singularity terms. All singularity terms are investigated in detail. The orders of singularities and the angular functions are calculated using eigenanalysis proposed in [17], and extended for piezoelectric materials in [10,11]. The intensities of singularities are calculated using the conservative integral based on Betti's reciprocal theorem. There were several studies that used the conservative integral to calculate the intensities of singularity or stress intensity factors. For example, [18–20] used this method for crack problems, and [21–25] used this method for dissimilar material bonded joints or interface corners. Those studies proved that the conservative integral can be used to accurately calculate the intensity of singularity. Furthermore, the conservative integral has the major advantage that the intensity of singularity for each term of singularity can be calculated individually.

In the case of the multi-term of singularities, the value of the intensity of singularity for each term is required for summarizing the singularity in an equation or matrix form, such as the unified singular stress equation proposed in [15]. Results obtained by using the conventional finite element analysis (FEA) are stress and electric displacement values, not easily separating each singularity term. This means that the conservative integral is useful in arranging the results in the unified form. In addition, the previous studies [15,16] revealed that for cases of applied tensile loading, the intensity of singularity for the first term of singularity generally had the largest value, making stress fields to be estimated solely using first term singularity outcomes. However, the results might be different for applied shear loading or mixed-mode conditions.

In Section 2, the analytical formulas are presented. The numerical analysis is described in detail in Section 3. This section is divided into 4 subsections. The analytical models and boundary conditions are presented in Section 3.1. The results of the orders of singularities and the angular functions, for both at the vertices and along the singular lines, are described in Section 3.2. In Section 3.3, the results of the intensities of singularities, for both at the vertices and along the singular lines, are presented. In Section 3.4, distributions of stresses and electric displacements are presented and compared to the results obtained using the conventional FEA with mesh refinement to demonstrate the accuracy of the conservative integral. Finally, conclusion is presented in Section 4.

2 Analytical formulas

2.1 Singularity equations for piezoelectric bonded joints

The general equations for asymptotic solutions around the singular point can be written as follows:

$$\sigma_{ij}(r, \theta, \phi) = \sum_{n=1}^{m} K_n \left(\frac{r}{L}\right)^{-\lambda_n} f_{ij}^{(n)}(\theta, \phi), \tag{1}$$

$$u_i(r, \theta, \phi) = \sum_{n=1}^{m} K_n \left(\frac{r^{1-\lambda_n}}{L^{-\lambda_n}}\right) g_i^{(n)}(\theta, \phi), \tag{2}$$

where the subscripts $i, j = r, \theta, \phi$ in the spherical coordinate system (Figure 1(a) and (b)). The length L is set to be the length of PZT-5H in the y-direction.

For piezoelectric material, the asymptotic solutions related to the electric properties are written as follows:

$$\sigma_{4j}(r, \theta, \phi) = \sum_{n=1}^{m} K_n \left(\frac{r}{L}\right)^{-\lambda_n} f_{4j}^{(n)}(\theta, \phi), \tag{3}$$

$$u_4(r, \theta, \phi) = \sum_{n=1}^{m} K_n \left(\frac{r^{1-\lambda_n}}{L^{-\lambda_n}}\right) g_4^{(n)}(\theta, \phi). \tag{4}$$

Following [15], the unified singular equation (for three terms of singularities) are written as follows:

$$[\boldsymbol{\sigma}(r, \theta, \phi)] = [\boldsymbol{f}(\theta, \phi)] \left[\left(\frac{r}{L}\right)^{-\boldsymbol{\lambda}}\right] [\boldsymbol{K}], \tag{5}$$

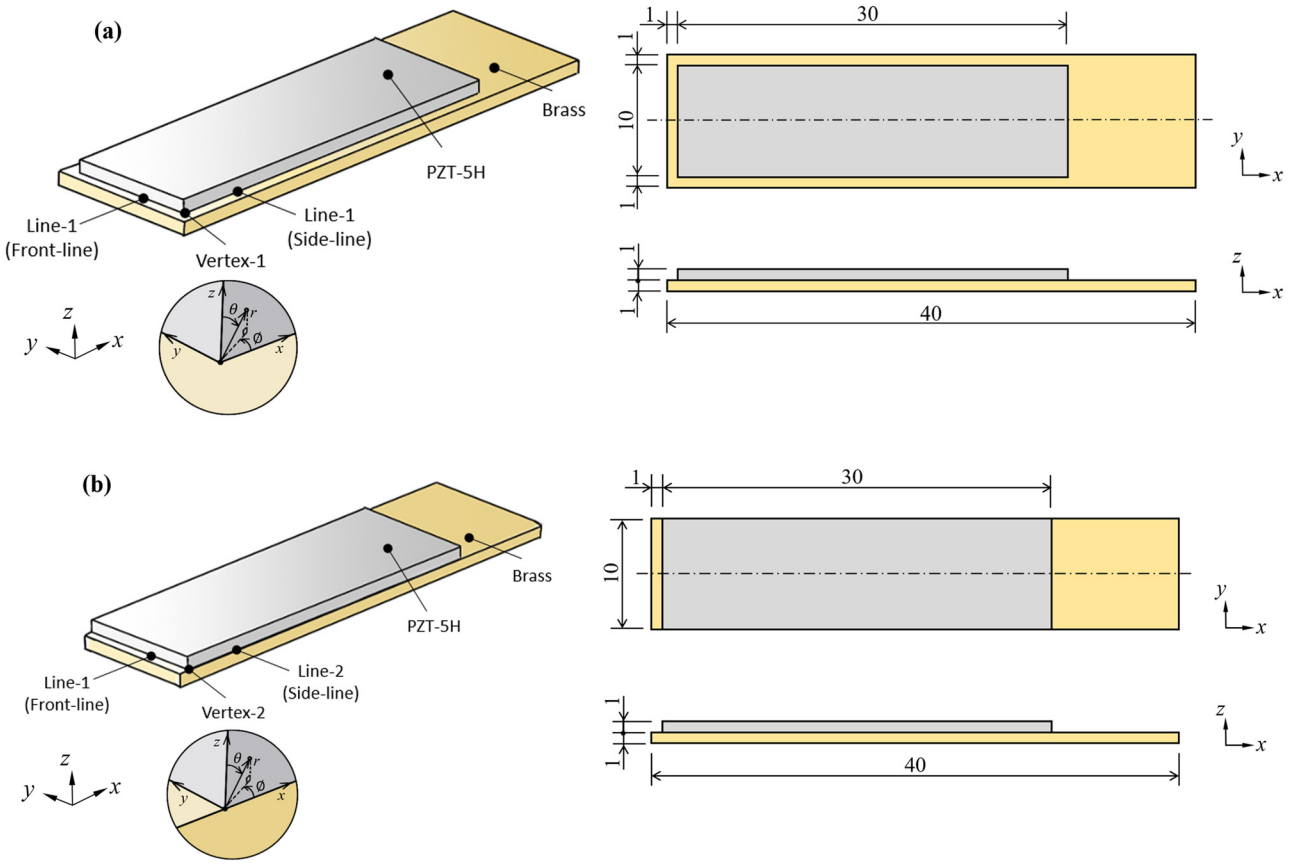

Figure 1: Analytical Models: (a) Model-1 and (b) Model-2.

where

$$[\boldsymbol{\sigma}(r,\theta,\phi)] = \begin{Bmatrix} \sigma_{rr}(r,\theta,\phi) \\ \sigma_{\theta\theta}(r,\theta,\phi) \\ \sigma_{\phi\phi}(r,\theta,\phi) \\ \tau_{r\theta}(r,\theta,\phi) \\ \tau_{r\phi}(r,\theta,\phi) \\ \tau_{\theta\phi}(r,\theta,\phi) \\ D_r(r,\theta,\phi) \\ D_\theta(r,\theta,\phi) \\ D_\phi(r,\theta,\phi) \end{Bmatrix},$$

$$[\boldsymbol{f}(\theta,\phi)] = \begin{bmatrix} f_{rr}^{(1)}(\theta,\phi) & f_{rr}^{(2)}(\theta,\phi) & f_{rr}^{(3)}(\theta,\phi) \\ f_{\theta\theta}^{(1)}(\theta,\phi) & f_{\theta\theta}^{(2)}(\theta,\phi) & f_{\theta\theta}^{(3)}(\theta,\phi) \\ f_{\phi\phi}^{(1)}(\theta,\phi) & f_{\phi\phi}^{(2)}(\theta,\phi) & f_{\phi\phi}^{(3)}(\theta,\phi) \\ f_{r\theta}^{(1)}(\theta,\phi) & f_{r\theta}^{(2)}(\theta,\phi) & f_{r\theta}^{(3)}(\theta,\phi) \\ f_{r\phi}^{(1)}(\theta,\phi) & f_{r\phi}^{(2)}(\theta,\phi) & f_{r\phi}^{(3)}(\theta,\phi) \\ f_{\theta\phi}^{(1)}(\theta,\phi) & f_{\theta\phi}^{(2)}(\theta,\phi) & f_{\theta\phi}^{(3)}(\theta,\phi) \\ f_{4r}^{(1)}(\theta,\phi) & f_{4r}^{(2)}(\theta,\phi) & f_{4r}^{(3)}(\theta,\phi) \\ f_{4\theta}^{(1)}(\theta,\phi) & f_{4\theta}^{(2)}(\theta,\phi) & f_{4\theta}^{(3)}(\theta,\phi) \\ f_{4\phi}^{(1)}(\theta,\phi) & f_{4\phi}^{(2)}(\theta,\phi) & f_{4\phi}^{(3)}(\theta,\phi) \end{bmatrix},$$

$$\left[\left(\frac{r}{L}\right)^{-\boldsymbol{\lambda}}\right] = \begin{bmatrix} \left(\frac{r}{L}\right)^{-\lambda_1} & 0 & 0 \\ 0 & \left(\frac{r}{L}\right)^{-\lambda_2} & 0 \\ 0 & 0 & \left(\frac{r}{L}\right)^{-\lambda_3} \end{bmatrix}, \quad [\boldsymbol{K}] = \begin{Bmatrix} K_1 \\ K_2 \\ K_3 \end{Bmatrix}.$$

2.2 Method for calculating the order of singularity and the angular functions

Following [10,11], the eigenvalue analysis can be used to calculate the order of singularity, λ_n. The eigen equation is written as follows:

$$(p^2[A] + p[B] + [C])\{u\} = 0, \tag{6}$$

where [**A**], [**B**], and [**C**], are matrices composed of material properties. {**u**} is the eigenvector of displacement and electric potential. The eigenvector analysis is used to obtain the angular functions of the displacements and the electric potential, $g_i^{(n)}(\theta,\phi)$ and $g_4^{(n)}(\theta,\phi)$, shown in

Eqs (2) and (4). Next the stress–strain relation can be used to derive the angular functions of the stresses and the electric displacements, $f_{ij}^{(n)}(\theta, \phi)$ and $f_{4j}^{(n)}(\theta, \phi)$, shown in Eqs (1) and (3).

In this study, the orders of singularities are calculated at the vertex and the point on the singular line. The angular functions at the vertex for each order of singularity are normalized as follows:

$$f_{\theta\theta\text{vertex}}^{(1)}\left(\frac{\pi}{2}, \frac{\pi}{4}\right) = 1,\ f_{r\varnothing\text{vertex}}^{(2)}\left(\frac{\pi}{2}, \frac{\pi}{4}\right) = 1,\ f_{\theta\theta\text{vertex}}^{(3)}\left(\frac{\pi}{2}, \frac{\pi}{4}\right) = 1. \tag{7}$$

On the other hand, the angular functions at the point on the singular line are normalized as follows:

$$f_{\theta\theta\text{line}}^{(1)}\left(\frac{\pi}{2}, \frac{\pi}{2}\right) = 1,\ f_{r\varnothing\text{line}}^{(2)}\left(\frac{\pi}{2}, \frac{\pi}{2}\right) = 1,\ f_{\theta\theta\text{line}}^{(3)}\left(\frac{\pi}{2}, \frac{\pi}{2}\right) = 1. \tag{8}$$

(See [10,11] for details of this method for calculating the order of singularity and the angular functions.)

2.3 Method for calculating the intensity of singularity

The conservative integral for three-dimensional model was first proposed in [26]. This method was extended to calculate the intensity of singularity, K_n, at the vertex and along the singular line of the piezoelectric bonded joints in 15,16]. The conservative integral is written as follows:

$$\int_s (T'_i u_i - T_i u'_i)\mathrm{d}s = 0. \tag{9}$$

Following [15,16], the H-integral (the conservative integral) at the singular point is written as follows:

$$H = \int_{S_\Gamma} (\sigma'_{ij} u_i - \sigma_{ij} u'_i)\hat{n}_j \mathrm{d}s, \tag{10}$$

where S_Γ is an arbitrary surface area surrounding the singular point.

To solve Eq. (10), two sets of solutions, unprimed (σ_{ij}, u_i) and primed (σ'_{ij}, u'_i) solutions, are required. The unprimed solutions are defined to be the singular solutions obtained using the eigenanalysis as follows:

$$\sigma_{ij}^{(n)}(r, \theta, \phi) = K_n\left(\frac{r}{L}\right)^{-\lambda_n} f_{ij}^{(n)}(\theta, \phi), \tag{11}$$

$$u_i^{(n)}(r, \theta, \phi) = K_n\left(\frac{r^{1-\lambda_n}}{L^{-\lambda_n}}\right) g_i^{(n)}(\theta, \phi). \tag{12}$$

The primed solutions are defined to be complementary solutions with the order of singularity of $\lambda' = 3 - \lambda$. The primed solutions are written as follows:

$$\sigma_{ij}'^{(n)}(r, \theta, \phi) = C_n\left(\frac{r}{L}\right)^{-\lambda_{\prime n}} f_{ij}'^{(n)}(\theta, \phi), \tag{13}$$

$$u_i'^{(n)}(r, \theta, \phi) = C_n\left(\frac{r^{1-\lambda_{\prime n}}}{L^{-\lambda_{\prime n}}}\right) g_i'^{(n)}(\theta, \phi), \tag{14}$$

where C_n is derived by setting $H_{\Gamma_\varepsilon} \equiv K_n$, such that

$$C_n = \frac{1}{L^3 \int_\theta \int_\phi \{f_{ir}'^{(n)}(\theta, \phi) g_i^{(n)}(\theta, \phi) - f_{ir}^{(n)}(\theta, \phi) g_i'^{(n)}(\theta, \phi)\} \sin\theta \mathrm{d}\phi \mathrm{d}\theta}. \tag{15}$$

(See [15,16] for details of this method for calculating the intensity of the singularity at the vertex and at the point along the singular line, respectively.)

3 Numerical analysis

3.1 Analysis models

Two unimorph models are used in this analysis. The difference between two models is their side surface shape (Figure 1(a) and (b)). The material above the interface is PZT-5H with the poling direction in the z-axis. The material below the interface is brass. The vertices of the models are considered to be the intersection between two side surfaces (front-line and side-line). Each side surface is considered to be a dissimilar material bonded line. There are two types of bonded line used in these models:

1. Line-1 (or step surface) is the side surface where θ = 0–90° for PZT-5H and θ = 90–270° for brass (Figure 1(a)).
2. Line-2 (or flat surface) is the side surface where θ = 0–90° for PZT-5H and θ = 90–180° for brass (Figure 1(b)).

Model-1 is the model in which all side surfaces are Line-1. Vertex-1 is the vertex formed by two step surfaces (Line-1). Model-2 is the model in which one side is Line-1 and the other is Line-2. It means that Vertex-2 is the vertex in which Line-1 (front-line) intersects Line-2 (side-line). Dimensions for Model-1 and Model-2 are shown in Figure 1(a) and (b), respectively. The boundary conditions are shown in Figure 2. Both models are clamped at one end and free along the remainder of their length. The free end is applied with compression loading and deformed by 0.1 mm in the z-direction. The material properties are presented in Table 1.

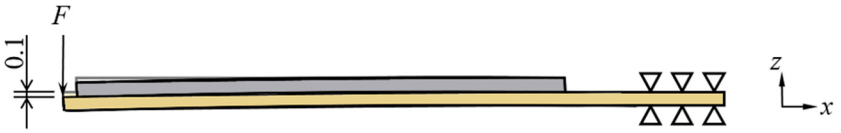

Figure 2: The boundary conditions.

Table 1: Material properties

		PZT-5H	Brass
Elastic constant, GPa	C_{11}	126	E = 100 GPa,
	C_{12}	55	v = 0.307
	C_{13}	53	
	C_{33}	117	
	C_{44}	35.3	
Piezoelectric constant, C/m^2	e_{31}	−6.5	
	e_{33}	23.3	
	e_{15}	17.0	
Dielectric constant, 10^{-10} C/Vm	χ_{11}	151	
	χ_{33}	130	

3.2 The orders of singularities and angular functions

The orders of the singularity at the vertices, $\lambda_{(v,n)}^{\text{vertex}}$ (where the subscripts v = 1, 2 represent Vertex-1 and Vertex-2, respectively. n is the n-term of singularity in descending order), are presented in Table 2. The results show that there are three-term of singularities at each vertex. The values of the orders of singularities of Vertex-1 for all terms are larger than that of Vertex-2.

Table 3 presents the orders of singularities along the singular line, $\lambda_{(l,n)}^{\text{line}}$ (where the subscripts l = 1, 2 represent Line-1 and Line-2, respectively). The results show that Line-2 is a non-singular line (the values of the order of singularity = 0).

Table 2: The orders of singularities at the vertices, $\boldsymbol{\lambda_{(v,n)}^{\text{vertex}}}$.

	$\boldsymbol{\lambda_{(v,1)}^{\text{vertex}}}$	$\boldsymbol{\lambda_{(v,2)}^{\text{vertex}}}$	$\boldsymbol{\lambda_{(v,3)}^{\text{vertex}}}$
Model-1 ($\lambda_{(1,n)}^{\text{vertex}}$)	0.575	0.211	0.109
Model-2 ($\lambda_{(2,n)}^{\text{vertex}}$)	0.371	0.208	0.038

Table 3: The orders of singularities along the singular line, $\boldsymbol{\lambda_{(l,n)}^{\text{line}}}$

	$\boldsymbol{\lambda_{(l,1)}^{\text{line}}}$	$\boldsymbol{\lambda_{(l,2)}^{\text{line}}}$	$\boldsymbol{\lambda_{(l,3)}^{\text{line}}}$
$\lambda_{(1,n)}^{\text{line}}$	0.459	0.324	0.096
$\lambda_{(2,n)}^{\text{line}}$	0.000	0.000	0.000

Following [16], the singularity at the vertex may be considered to be the combination of two singularities along the singular line (where two sides meet). That is, Vertex-1 is the combination of two singular lines, and Vertex-2 is the combination of one singular line and one non-singular line.

3.3 The intensities of singularities

3.3.1 The intensities of singularities at the vertices

The intensities of singularities at the vertices are calculated using the conservative integral together with the three-dimensional FEA. The FE models used to obtain the displacements and the electric potentials are shown in Figure 3(a) and (b) for Model-1 and Model-2, respectively. These models are symmetric about their centerline. Thus, the half-symmetry FE models are used. The intensities of singularities, $K_{(v,n)}^{\text{vertex}}$, are presented in Table 4. The results indicated that the values of intensities of singularities of Model-1 are larger than that of Model-2 for all singularity terms. However, some negative values may affect the magnitudes of stresses (See [15] for details of the conservative integral for the vertex).

3.3.2 The intensities of singularities along the singular lines

The intensities of the singularities at several points located on the singular lines are examined. For Model-1, there are two lines for analysis; whereas, there is solely one line (front-line) for Model-2 because Line-2 is considered to be the non-singular line ($\lambda_{(2,n)}^{\text{line}}$ = 0).

Examples of the FE models used to obtain the displacements and the electric potentials (for front-line at d = 3 mm) are presented in Figure 4(a) and (b) for Model-1 and Model-2, respectively.

The intensities of singularities at the points located on the singular lines are presented in Tables 5 and 6. The results of the front-line, $K_{(l,n)}^{F\text{-line}}$, at the points located at 1, 2, 3, and 4 mm from the vertices are presented in Table 5.

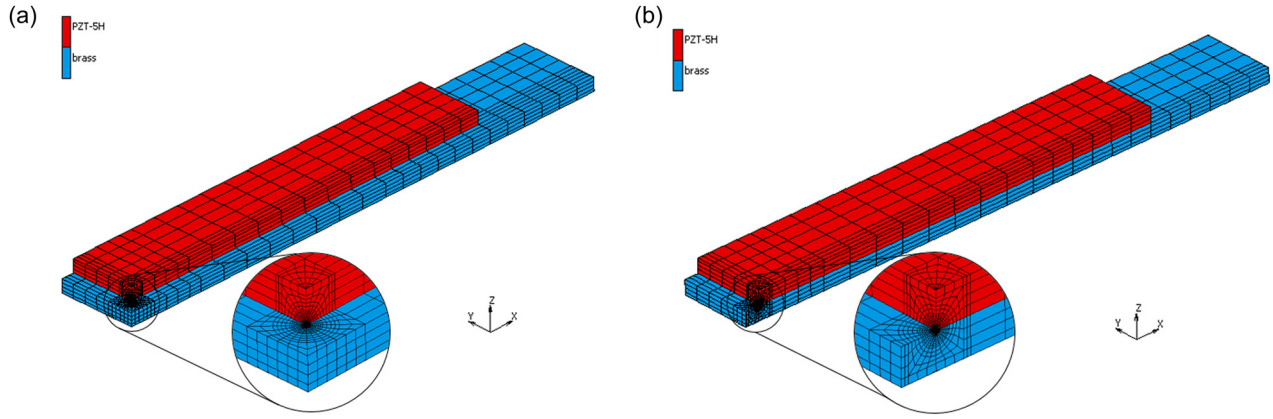

Figure 3: The FE models used to obtain the displacements and the electric potentials: (a) Vertex-1 and (b) Vertex-2.

Table 4: The intensities of singularities at the vertices, $K^{\text{vertex}}_{(v,n)}$

	$K^{\text{vertex}}_{(v,1)}$	$K^{\text{vertex}}_{(v,2)}$	$K^{\text{vertex}}_{(v,3)}$
Vertex-1 ($K^{\text{vertex}}_{(1,n)}$)	680.42	−690.95	−176.65
Vertex-2 ($K^{\text{vertex}}_{(2,n)}$)	668.23	−122.96	41.01

The values of the intensities of singularities of Model-1 at each point are similar to that of Model-2; in addition, the values of $K^{F\text{-line}}_{(l,1)}$ (the first term) are the largest within three singularity terms. The results of the side-line, $K^{s\text{-line}}_{(1,n)}$, at the points located at 1, 2, 3, and 4 mm from Vertex-1 (Model-1) are presented in Table 6. The results are different from that of the front-line; in other words, the values of $K^{s\text{-line}}_{(1,2)}$ (the second term) are larger than that of $K^{s\text{-line}}_{(1,1)}$ (the first term). This may be caused by the mixed-mode conditions. It may be noted that it is necessary to calculate the intensity of singularity for all singularity terms because the maximum value may not be the value of the first term of singularity.

3.4 Distributions of stresses and electric displacements

The results in Section 3.3 show that some values of intensities of singularities are negative, and some are positive. Therefore, it is difficult to compare the magnitudes of stresses or electric displacements using only the orders or the intensities of singularities since there are multi-terms of singularities. To evaluate the results between two models, the distribution of the stresses and electric displacements are presented by substituting the intensities of singularities, K, (the results in Section 3.3) with the orders of singularities, λ, and the angular functions, $f_{ij}(\theta, \phi)$, (the results in Section 3.2) in the unified singular equation (Eq. (5)).

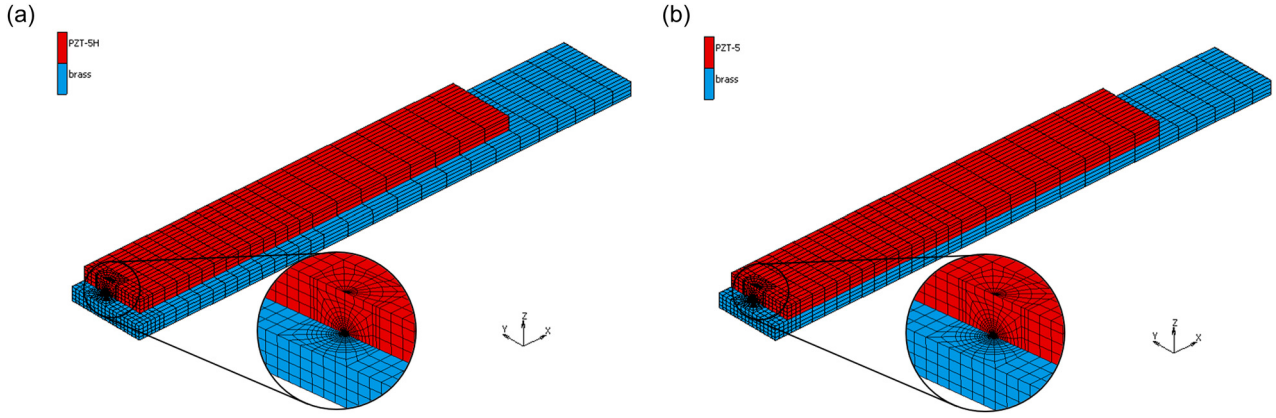

Figure 4: The FE models used to obtain the displacements and the electric potentials for front-line at d = 3 mm: (a) Model-1 and (b) Model-2.

Table 5: The intensities of singularities along the front-line, $K^{F\text{-line}}_{(l,n)}$

	d (mm)	$K^{F\text{-line}}_{(l,1)}$	$K^{F\text{-line}}_{(l,2)}$	$K^{F\text{-line}}_{(l,3)}$
$K^{F\text{-line}}_{(1,n)}$	1	483.33	53.80	186.48
	2	388.01	31.96	178.70
	3	354.92	20.39	187.77
	4	341.41	6.38	191.50
$K^{F\text{-line}}_{(2,n)}$	1	487.50	30.01	172.35
	2	391.14	27.43	180.57
	3	346.50	19.55	188.53
	4	326.75	6.17	190.61

Table 6: The intensities of singularities along the side-line, $K^{S\text{-line}}_{(l,n)}$

	d (mm)	$K^{S\text{-line}}_{(l,1)}$	$K^{S\text{-line}}_{(l,2)}$	$K^{S\text{-line}}_{(l,3)}$
$K^{S\text{-line}}_{(1,n)}$	1	−27.27	−252.61	−66.26
	2	−26.67	−248.95	−66.61
	3	−8.96	−250.46	−39.22
	4	2.21	−250.35	−31.94

Figures 5 and 6 present the distribution of stresses at the vertices with respect to the distance from r. The normal stresses, $\sigma_{\theta\theta}$, at ϕ = 45° and θ = 45° and 90° are presented in Figure 5(a) and (b) for Vertex-1 and Vertex-2, respectively. The shear stresses, $\tau_{r\theta}$, at ϕ = 45° and θ = 45° and 90° are presented in Figure 6(a) and (b) for Vertex-1 and Vertex-2, respectively. According to these figures, the values of stresses of Vertex-1 are much larger than those of Vertex-2. Comparing between absolute values of normal stresses and shear stresses, the values of normal stresses, $\sigma_{\theta\theta}$, at ϕ = 45° and θ = 90° are larger than the values of shear stresses, $\tau_{r\theta}$ for both vertices, whereas, at θ = 45°, $\sigma_{\theta\theta}$ is smaller than $\tau_{r\theta}$.

Figures 7 and 8 present the distribution of stresses at the interface, θ = 90°, with respect to ϕ for r = 0.01 and 0.1 mm. The normal stresses, $\sigma_{\theta\theta}$, are presented in Figure 7(a) and (b) for Vertex-1 and Vertex-2, respectively. According to these figures, the value of stresses increases as it approaches the singular line (Figure 7(b) clearly shows that at ∅ = 0°, that is the non-singular line, the values of stresses are small). The shear stresses, $\tau_{r\theta}$,

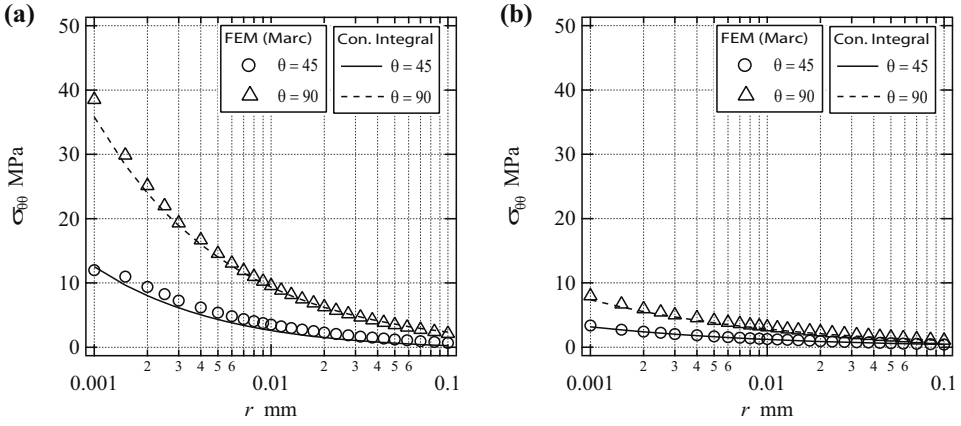

Figure 5: Distribution of normal stresses, $\sigma_{\theta\theta}$, at ϕ = 45° and θ = 45° and 90° with respect to r: (a) Vertex-1 and (b) Vertex-2.

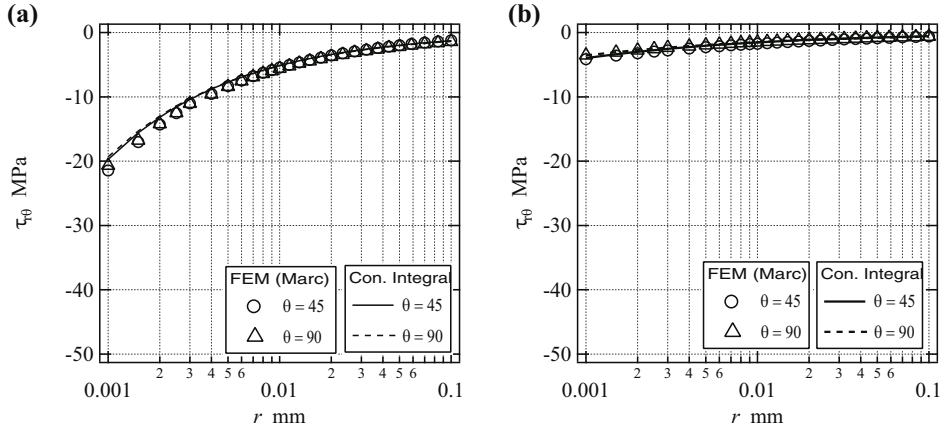

Figure 6: Distribution of shear stresses, $\tau_{r\theta}$, at ϕ = 45° and θ = 45° and 90° with respect to r: (a) Vertex-1 and (b) Vertex-2.

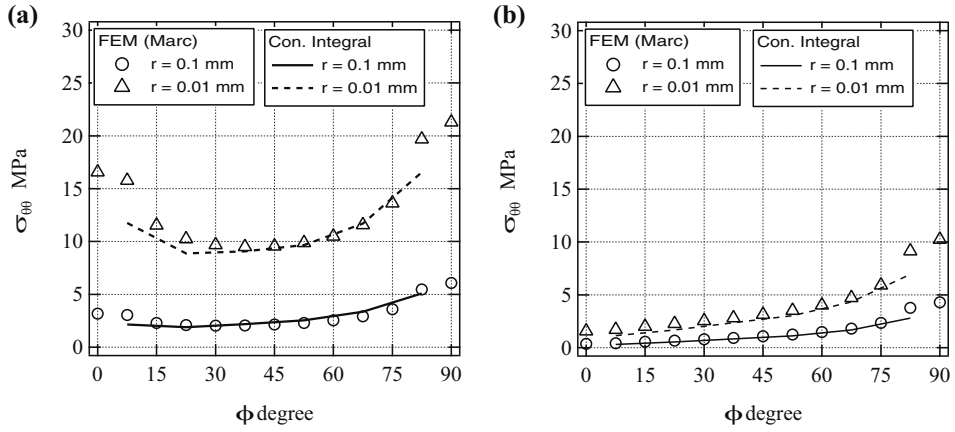

Figure 7: Distribution of normal stresses, $\sigma_{\theta\theta}$, at the interface, $\theta = 90°$, with fixed r at 0.01 and 0.1 mm: (a) Vertex-1 and (b) Vertex-2.

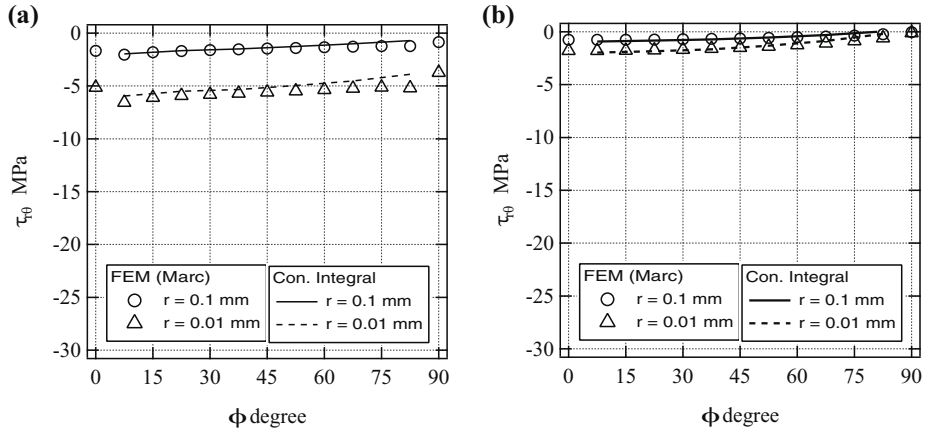

Figure 8: Distribution of shear stresses, $\tau_{r\theta}$, at the interface, $\theta = 90°$, with fixed r at 0.01 and 0.1 mm: (a) Vertex-1 and (b) Vertex-2.

are presented in Figure 8(a) and (b) for Vertex-1 and Vertex-2, respectively. The results of shear stresses are different from that of normal stresses. For both vertices, the value of stresses does not increase as it approaches the singular line. However, the value of shear stresses, $\tau_{r\theta}$, of Vertex-1 is much larger than that of Vertex-2.

Figure 9(a) and (b) present the distribution of electric displacements, D_θ, at $\phi = 45°$ and $\theta = 45°$ and 90° with respect to r for Vertex-1 and Vertex-2, respectively. In addition, the distribution of electric displacement, D_θ, at the interface, $\theta = 90°$, with respect to ϕ for $r = 0.01$ and 0.1 mm, is presented in Figure 10(a) and (b), for Vertex-1 and Vertex-2, respectively. Similar to the stresses, the values of electric displacements of Vertex-1 are much larger than that of Vertex-2, and the values of the electric displacements increase as it gets closer to the singular line. These results confirm that the singularities effect to electric fields and the electric displacements increase as it approaches the singular line.

Figures 11–14 present the results along the front-line at $d = 3$ mm. The distribution of normal stresses, $\sigma_{\theta\theta}$, at $\phi = 90°$ and $\theta = 45°$ and 90° with respect to r is presented in Figure 11(a) and (b), and $\sigma_{\theta\theta}$ at the interface, $\theta = 90°$, with respect to ϕ for $r = 0.01$ and 0.1 mm, are presented in Figure 12(a) and (b), for Model-1 and Model-2, respectively. According to these results, the values of the stresses along the front-line of Model-1 are similar to those of Model-2, which corresponds to that of the intensities of singularities. Next the results of the electric displacements for the same paths as the stresses are shown in Figures 13 and 14. The results of the electric displacements are in the same trend as the results of stresses.

In addition to the results obtained using the conservative integral, the distribution of stresses and the electric displacements obtained using the conventional FEM with mesh refinement (0.0005 mm is the smallest element size in the r-direction) is also plotted in Figures 5–14 for comparison. The results are in good agreement. Therefore,

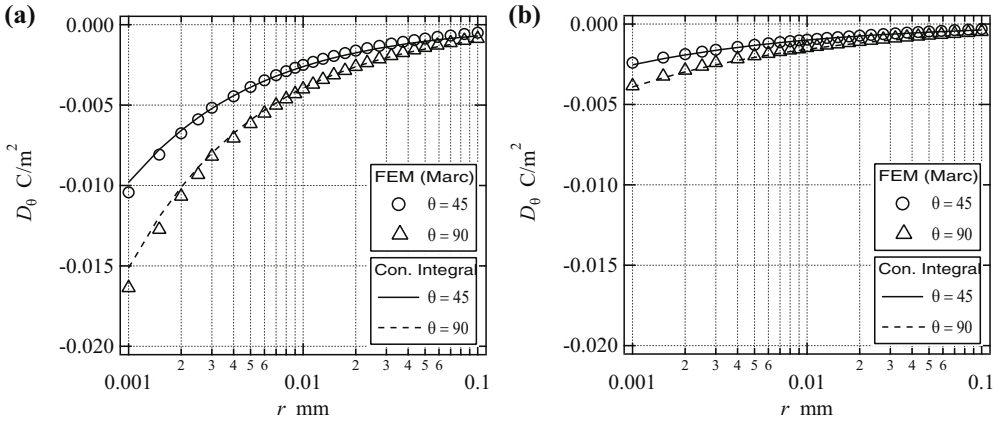

Figure 9: Distribution of electric displacements, D_θ, at $\phi = 45°$ and $\theta = 45°$ and 90° with respect to r: (a) Vertex-1 and (b) Vertex-2.

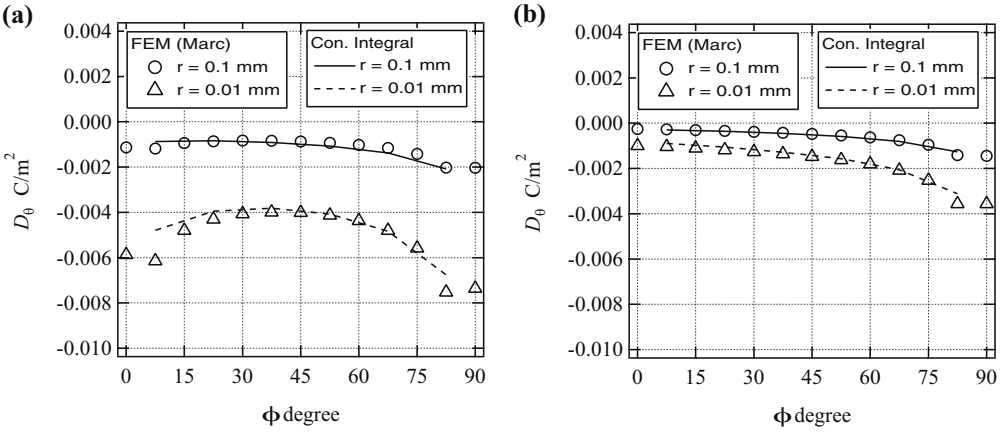

Figure 10: Distribution of electric displacements, D_θ, at the interface, $\theta = 90°$, with fixed r at 0.01 and 0.1 mm: (a) Vertex-1 and (b) Vertex-2.

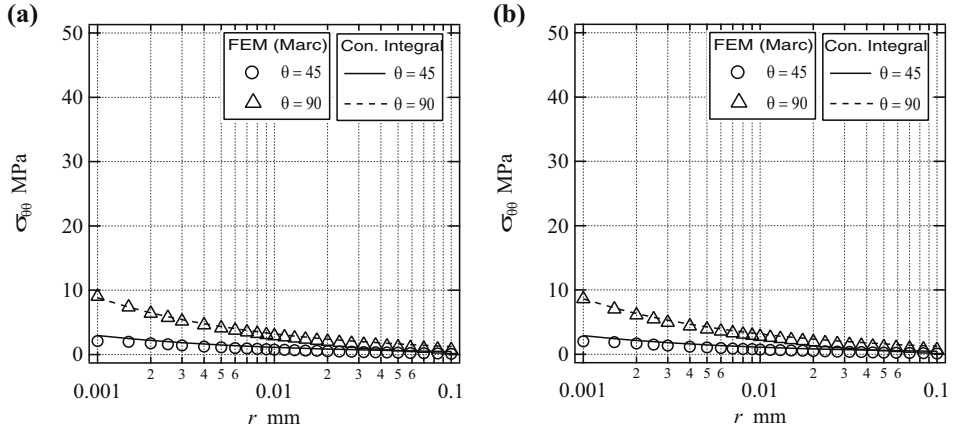

Figure 11: Distribution of normal stresses, $\sigma_{\theta\theta}$, at $\phi = 90°$ and $\theta = 45°$ and 90° with respect to r on the singular line (front-line at $d = 3$ mm): (a) Model-1 and (b) Model-2.

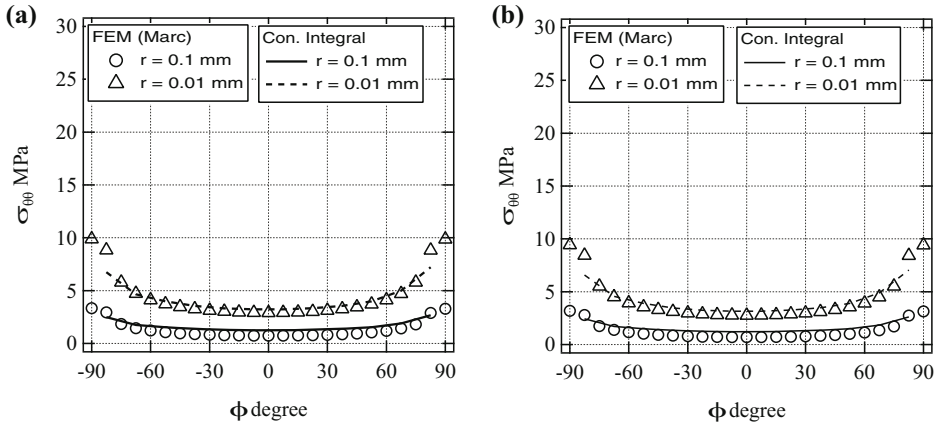

Figure 12: Distribution of stresses, $\sigma_{\theta\theta}$, at the interface, $\theta = 90°$, with fixed r at 0.01 and 0.1 mm on the singular line (front-line at $d = 3$ mm): (a) Model-1 and (b) Model-2.

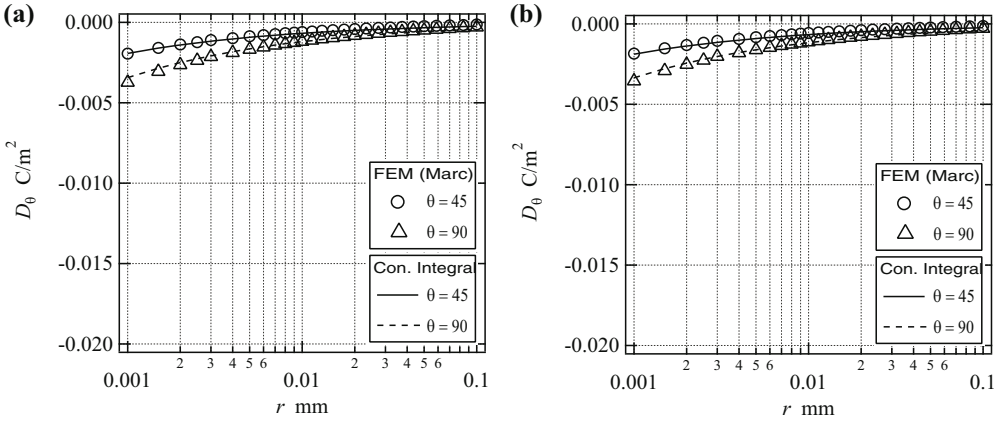

Figure 13: Distribution of electric displacements, D_θ, at $\phi = 90°$ and $\theta = 45°$ and 90° with respect to r on the singular line (front-line at $d = 3$ mm): (a) Model-1 and (b) Model-2.

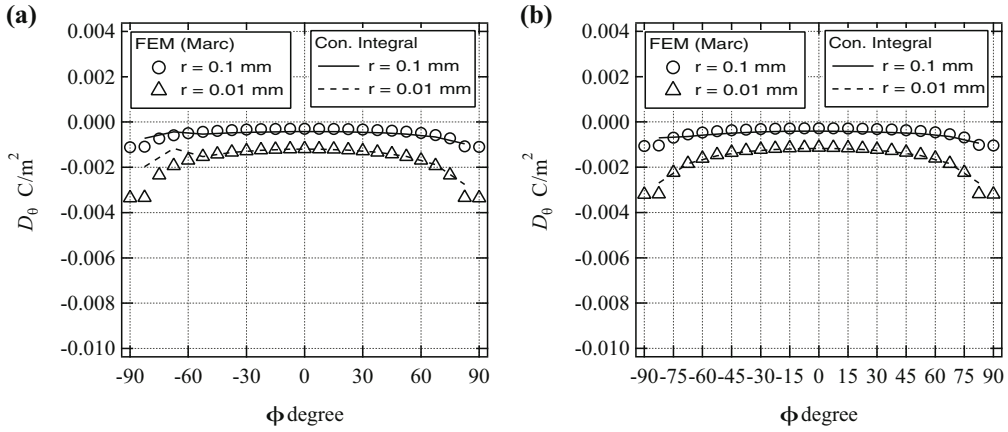

Figure 14: Distribution of electric displacements, D_θ, at the interface, $\theta = 90°$, with fixed r at 0.01 and 0.1 mm on the singular line (front-line at $d = 3$ mm): (a) Model-1 and (b) Model-2.

accurate intensities of singularities can be obtained using the conservative integral. In addition, the singular stresses and electric displacements can be expressed by the unified singular equation (Eq. (5)).

4 Conclusion

In this study, the orders of singularities and the intensities of singularities at the vertices and along the free edges (the singular lines) of the interface corners of piezoelectric-brass unimorphs were obtained. Two models which differ in bonded shape were investigated. These models consist of multi-terms of singularity, and were applied the mixed-mode conditions. The conclusions are as follows:

1. The results revealed that the singularities of the piezoelectric bonded joints affect the electric fields. The magnitude of electric displacements increases dramatically as it approached the vertices and the singular lines.
2. The results of the orders of singularities and the intensities of the singularities revealed that, for three-dimensional models, the stress singularity characteristics at the vertex might be described as a function of the singularities along the side surfaces of the interface (the singular lines). Comparing between two models, Vertex-1 (two singular side surfaces) generated much larger stresses and electric displacements than that of Vertex-2 (one singular side surface).
3. The cases of multi-terms of singularity with applied mixed-mode boundary conditions, it is necessary to calculate the intensity of singularity for the second-term and the third-term of singularity because the maximum intensity of singularity might not be the value of the first-term of singularity. Furthermore, the results (all three terms) could be expressed by the unified singular equation. It was found that accurate intensities of singularities can be calculated using the conservative integral.

In summary, these findings clarify the understanding of singularity at interface corners of piezoelectric-brass unimorphs and may be used as references for developing relevant piezoelectric devices.

Nomenclature

d	distance from the vertex
f_{ij}	angular function of stress
f_{4j}	angular function of electric displacement
g_i	angular function of displacement
g_4	angular function of electric potential
K_n	intensity of singularity
L	model length
m	number of singularity term
p	eigenvalue ($p = 1 - \lambda$)
r	distance from the singular point
S	integral contour
T_i	tractions of the singular fields
T_i'	tractions of the complementary fields
T_4	electric displacement with the outward unit vector ($T_4 = \sigma_{4j}\hat{n}_j$) of the singular fields
T_4'	electric displacement of the complementary fields
u_i	displacements of the singular fields
u_i'	displacements of the complementary fields
u_4	electric potentials of the singular fields
u_4'	electric potentials of the complementary fields
λ_n	order of stress singularity
σ_{ij}	stress tensor
σ_{4j}	electric displacement

Funding information: This work was supported by Thailand Science Research and Innovation and National Research Council of Thailand (Grant No. MRG6280092).

Author contributions: All authors have accepted responsibility for the entire content of this manuscript and approved its submission.

Conflict of interest: Authors state no conflict of interest.

References

[1] APC International Ltd. Piezoelectric ceramics: Principles and Applications. 2nd ed. APC International; 2011.
[2] Shang F, Kuna M, Abendroth M. Finite element analyses of three-dimensional crack problems in piezoelectric structures. Eng Fract Mech. 2003;70(2):143–60.
[3] Banks-Sills L, Motola Y, Shemesh L. The M-integral for calculating intensity factors of an impermeable crack in a piezoelectric material. Eng Fract Mech. 2008;75:901–25.
[4] Motola M, Banks-Sills L. M-integral for calculating intensity factors of cracked piezoelectric materials using the exact boundary conditions. J Appl Mech. 2009;76:1–9.
[5] Lei J, Zhang C. Time-domain BEM for transient interfacial crack problems in anisotropic piezoelectric bi-materials. Int J Fract. 2012;174:163–75.
[6] Yu T, Bui TQ, Liu P, Zhang Ch, Hirose H. Interfacial dynamic impermeable cracks analysis in dissimilar piezoelectric

materials under coupled electromechanical loading with the extended finite element method. Int J Solids Struct. 2015;67–68:205–18.
[7] Xu XL, Rajapakse RK. On singularities in composite piezoelectric wedges and junctions. Int J Solids Struct. 2000;37(23):3253–75.
[8] Xu JQ, Mutoh Y. Singularity at the interface edge of bonded transversely isotropic piezoelectric dissimilar materials. JSME Int J Ser A Solid Mech Mater Eng. 2001;44:556–66.
[9] Chen CD. On the singularities of the thermo-electro-elastic fields near the apex of a piezoelectric bonded wedge. Int J Solids Struct. 2006;43:957–81.
[10] Islam MS, Koguchi H. Characteristics of singular stress distribution at a vertex in transversely isotropic piezoelectric dissimilar material joints. J Solid Mech Mater Eng. 2010;4(7):1011–26.
[11] Islam MS, Koguchi H. Analysis of singularity at a vertex in 3D transversely isotropic piezoelectric single-step bonded joints with various thicknesses by boundary element method. J Solid Mech Mater Eng. 2012;6:844–59.
[12] Hirai H, Chiba M, Abe M, Ikeda T, Miyazaki N. Stress intensity factor analysis of an interfacial corner between piezoelectric bimaterials using the H-integral method. Eng Fract Mech. 2012;82:60–72.
[13] Cheng CZ, Yao SL, Han ZL, Recho N, Niu ZR. Evaluation of the singularity exponents and characteristic angular functions for piezoelectric V-notches under in plane and out of plane conditions. Theor Appl Fract Mech. 2015;76:50–9.
[14] Zhenhuan Z, Zhenting Y, Wang X, Xiong Y, Chenghui X, Xinsheng X. Evaluation of electroelastic singularity of finite-size V-notched one-dimensional hexagonal quasicrystalline bimaterials with piezoelectric effect. Theor Appl Fract Mech. 2019;100:139–53.
[15] Luangarpa C, Koguchi H. Evaluation of intensities of singularity at three-dimensional piezoelectric bonded joints using a conservative integral. Eur J Mech A/Solids. 2018;72:198–208.
[16] Luangarpa C, Koguchi H. Singular stresses at a vertex and along a singular line in three-dimensional piezoelectric bonded joints. J Appl Comput Mech. 2020;6:1364–70.
[17] Pageau SS, Biggers SB, Jr. Finite element evaluation of free-edge singular stress fields in anisotropic materials. Int J Numer Meth Eng. 1995;38:2225–39.
[18] Stern M, Becker E, Dunham R. A contour integral computation of mixed-mode stress intensity factors. Int J Fract. 1976;7:125–32.
[19] Sinclair GB, Okajima M, Griffin JH. Path independent integrals for computing stress intensity factors at sharp notches in elastic plates. Int J Numer Methods Eng. 1984;20:999–1008.
[20] Carpenter WC. Calculation of fracture mechanics parameters for a general corner. Int J Fract. 1984;24:45–58.
[21] Hwu C, Kuo TL. A unified definition for stress intensity factors of interface corners and cracks. Int J Solids Struct. 2007;44:6340–59.
[22] Banks-Sills L. A conservative integral for determining stress intensity factors of a bimaterial strip. Int J Fract. 1997;86:385–98.
[23] Banks-Sills L, Sherer A. A conservative integral for determining stress intensity factors of a bimaterial notch. Int J Fract. 2002;115:1–26.
[24] Nomura Y, Ikeda T, Miyazaki N. Stress intensity factor analysis of a three-dimensional interfacial corner between anisotropic bimaterials under thermal stress. Int J Solids Struct. 2010;47:1775–84.
[25] Kuo TL, Hwu C. Multi-order stress intensity factors along three-dimensional interface corners. J Appl Mech. 2010;77(3):1–12.
[26] Luangarpa C, Koguchi H. Analysis of a three-dimensional dissimilar material joint with one real singularity using a conservative integral. Int J Solids Struct. 2014;51:2908–19.